Resolving the large scale spectral variability of the luminous Seyfert 1 galaxy 1H 0419-577

K.A.Pounds[1], J.N.Reeves[2,3], K.L.Page[1], P.T.O'Brien[1]

kap@star.le.ac.uk

ABSTRACT

An *XMM-Newton* observation of the luminous Seyfert 1 galaxy 1H 0419-577 in September 2002, when the source was in an extreme low-flux state, found a very hard X-ray spectrum at 1–10 keV with a strong soft excess below ~1 keV. Comparison with an earlier *XMM-Newton* observation when 1H 0419-577 was 'X-ray bright' indicated the dominant spectral variability was due to a steep power law or cool Comptonised thermal emission. Four further *XMM-Newton* observations, with 1H 0419-577 in intermediate flux states, now support that conclusion, while we also find the variable emission component in intermediate state difference spectra to be strongly modified by absorption in low ionisation matter. The variable 'soft excess' is seen to be an artefact of absorption of the underlying continuum while the 'core' soft emission is attributed to recombination in an extended region of more highly ionised gas. This new analysis underlines the importance of fully accounting for absorption in characterising AGN X-ray spectra.

Subject headings: X-ray astronomy:XMM-Newton:Seyfert galaxies:1H0419-577,LB 1727

1. Introduction

1H 0419-577 (also known as LB 1727) is a radio-quiet (8.4 GHz flux ~3 mJy; Brissenden et al.1987) Seyfert galaxy at a redshift z~0.104 and one of the brightest AGN in the extreme

[1]Department of Physics and Astronomy, University of Leicester, Leicester LE1 7RH, UK

[2]Laboratory for High Energy Astrophysics, Code 662, NASA Goddard Space Flight Center, Greenbelt, MD 20771, USA

[3]Universities Space Research Association

ultra-violet, being detected by both the *ROSAT* Wide Field Camera (Pye et al. 1995) and *EUVE* (Marshall et al. 1995). Optical spectra from the AAT (Turner et al. 1999) and ESO (Guainazzi et al. 1998) showed 1H 0419-577 to be a typical broad line Seyfert 1 with a strong Big Blue Bump (BBB). It has been widely studied at X-ray energies and found to exhibit an unusual degree of spectral variability. A short pn-camera observation early in the *XMM-Newton* programme reported a 'typical' Seyfert 1 X-ray spectrum with a power law of photon index $\Gamma\sim1.9$ together with a strong soft excess (Page et al. 2002). Using the Hβ line width from Grupe et al. (2004) and the relationship with black hole mass of Kaspi et al. (2000), we estimate a mass of $1.3 \times 10^8 M_\odot$ for 1H 0419-577. The [OIII] 5007Å line width measure of the stellar velocity dispersion (Nelson 2000) gives a very similar figure.

To improve the X-ray data on 1H 0419-577 a new series of 5 *XMM-Newton* observations was carried out, at approximately 3-monthly intervals over the period September 2002 to September 2003. The first of those new observations, when 1H 0419-577 was found to be in an extremely faint state, has been reported in Pounds et al. (2004); hereafter Paper 1. Three points of particular note resulting from that first new *XMM-Newton* observation of 1H 0419-577 were: (1) an unusually hard (flat) power law fit ($\Gamma\sim1.0$) to the EPIC data over the 2–10 keV band also exhibited curvature indicative of an extreme relativistic Fe K emission line or partial covering of the continuum by a substantial column of 'cold' gas; (2) although the RGS features were faint, the unambiguous detection of emission lines of OVII and OVIII provided clear evidence for an extended region of photo-ionised gas in the nucleus of 1H 0419-577; (3) a comparison of the raw EPIC data with data obtained in December 2000, when 1H 0419-577 was considerably brighter in the X-ray band, showed that the large-scale spectral variability in 1H 0419-577 could be described by a variable, steep ($\Gamma\sim2.5$) power law component.

In the present paper we analyse the remaining 4 observations from the new *XMM-Newton* campaign (in December 2002, March, June and September 2003), which together explore the X-ray spectrum of 1H 0419-577 over a range of flux states lying between the extremes of December 2000 and September 2002.

2. Observations and X-ray data

The new observations took place on 27 December 2002 (orbit 558), 30 March (orbit 605), 25 June (orbit 649) and 16 September (orbit 690) in 2003, with on-target exposures of $\sim$10.2 ksec, $\sim$13.9 ksec, $\sim$13.1 ksec and $\sim$13.9 ksec, respectively. X-ray data were available throughout each observation from the EPIC pn (Strüder et al. 2001) and MOS (Turner et al. 2001) cameras, and the Reflection Grating Spectrometer/RGS (den Herder et al.

2001). These new data add to the earlier *XMM-Newton* observations of 1H 0419-577 on 4 December 2000 (orbit 181) and 5 September 2002 (orbit 512) when the source was found to be in historically high and low flux states, respectively. Those earlier observations have been reported in Page et al. (2002) and in Paper 1.

EPIC data were initially screened with the XMM SAS v5.4 software and events corresponding to patterns 0-4 (single and double pixel events) were selected for the pn data and patterns 0-12 for MOS1 and MOS2, the latter then being combined. A low energy cut of 300 eV was applied to all EPIC data and known hot or bad pixels were removed. Source counts were obtained from a circular region of 45″ radius centred on 1H 0419-577, with the background being taken from a similar region offset from, but close to, the source. The X-ray light curve of 1H 0419-577 was essentially flat throughout each observation and the background rate was low (except in orbit 558, when noisy data were edited out). We therefore integrated each data set for spectral analysis. Individual EPIC spectra were binned to a minimum of 100 counts per energy bin to facilitate use of the χ^2 minimalisation technique in spectral fitting and ensure adequate statistics in the 5–10 keV band. Spectral fitting was based on the Xspec package (Arnaud 1996) and all fits included absorption due to the line-of-sight Galactic column $N_H = 2 \times 10^{20}\mathrm{cm}^{-2}$. Errors are quoted at the 90% confidence level ($\Delta\chi^2 = 2.7$ for one interesting parameter).

We were fortunate to observe 1H 0419-577 in widely differing flux states, ranging conveniently between the low and high flux state observations reported previously. Figure 1 shows the background-subtracted (pn camera) spectra for all 6 observations compared with a mean power law fit (at 2–10 keV) of Γ=1.73. The plot shows very clearly that the largest flux variation occurs in the soft X-ray band, with all spectra converging above $\sim$5 keV. The only significance we would claim for the mean power law fit is in the spectral index being close to the 'canonical' value for Seyfert 1 galaxies (for fits excluding reflection), suggesting that this unusually variable AGN has an *average* X-ray spectrum typical of the class. Retaining our previous descriptions of the orbit 181 and 512 data as, respectively, 'high' and 'low' flux states, we now define orbit 558 as 'mid-low', orbit 605 as 'mid-high' and group orbits 649 and 690 together to give a well-defined 'intermediate' flux state spectrum.

In the following analysis spectral parameters are quoted in the rest frame of 1H 0419-577 while figures (except fig. 10) retain the observed photon energy scale.

3. Spectral fitting of the intermediate flux state EPIC data

We began the EPIC spectral analysis in the conventional way by fitting a power law over the hard X-ray (2–10 keV) band, aiming thereby to minimise the effects of soft X-ray emission and/or low energy absorption. This fit yielded a photon index of Γ=1.60±0.01 (pn) and Γ=1.55±0.02 (MOS). Statistically, the simple power law fit was quite good, with χ^2 of 393 for 357 degrees of freedom (dof). The most obvious residual spectral feature is a weak emission line observed just below ∼6 keV (figure 2a). The addition of a gaussian emission line improved the fit (to χ^2 = 373/353 dof), with a line energy (in the AGN rest-frame) of 6.25±0.12 keV, rms width σ=320±150 eV, flux = 1.5±0.6×10^{-5} ph s^{-1} cm^{-2}, and EW = 100±40 eV.

Extending this spectral fit to 0.3 keV revealed the strong excess below ∼1 keV (figure 2b). The addition of blackbody components of kT ∼110 eV and kT ∼250 eV modelled the soft excess quite well, but it was necessary to add (ad hoc) absorption edges at ∼0.62 keV (τ∼0.22), ∼0.74 keV (τ∼0.26) and ∼0.90 keV (τ∼0.10) to achieve a statistically acceptable fit (χ^2 = 825/783 dof). Figure 3 reproduces this 'conventional' fit to the intermediate flux level data for 1H 0419-577 which we note has model parameters typical for a luminous Seyfert 1 galaxy.

The above spectral fitting allowed the mean X-ray fluxes of the intermediate state spectrum of 1H 0419-577 to be derived. These were: 5.9 × 10^{-12} erg s^{-1} cm^{-2} (0.3–1 keV), 3.0×10^{-12} erg s^{-1} cm^{-2} (1–2 keV), and 1.05×10^{-11} erg s^{-1} cm^{-2} (2–10 keV). Combining these fluxes yields an 'intermediate state' 0.3–10 keV luminosity for 1H 0419-577 of 4.3 × 10^{44} erg s^{-1} (H_0 = 75 $km s^{-1} Mpc^{-1}$).

4. An alternative spectral fit to the intermediate flux state spectrum

Our main aim in the present study is to better understand the large scale spectral variability of 1H 0419-577 - and thereby of AGN more generally. In Paper 1 we found that the difference spectrum between extreme high and low state EPIC pn data (the high flux difference spectrum) could be well fitted by a power law of Γ∼2.5, steepening to ∼2.7 above ∼2 keV. This simple fit suggested that the low state spectrum (hard power law plus soft excess) might represent a non-varying 'core' emission, leaving the main spectral change to be represented by the variable flux power law component. To further explore that possibility we now re-analyse the new intermediate flux state EPIC data, after subtracting the September 2002 data, to yield the intermediate state difference spectrum.

We find the resulting intermediate state difference spectrum is similar to the high state

difference spectrum, with a mean 0.3-10 keV power law index of $\Gamma\sim2.41$ (pn), steepening to ~2.85 when fitted above ~2 keV. However, the fit is much less good (χ^2 = 1174/799 dof), due to a broad deficit of flux at $\sim$0.5–1 keV (figure 4a). If the large-scale spectral variability in 1H 0419-577 is indeed well modelled by a steep, variable flux power law, as proposed in our previous analysis of the high state difference spectrum (Paper 1), the new data suggest the variable emission component is modified by absorption in intermediate flux states. To model that possibility we then compared the intermediate state difference spectrum with a power law plus a photoionised absorber, represented by XSTAR (Kallman et al. 1996). Here, the absorption is compared with a grid of ionised absorbers, with column density, ionisation parameter $\xi(= L/nr^2$, where n is the gas density at a distance r from the ionising source of luminosity L) and outflow (or inflow) velocity as variable parameters. All abundant elements from C to Fe are included, with the relative abundances as further variable parameters. The resulting fit was good (χ^2 of 839/790), with a column density $N_H\sim4\times10^{21}\mathrm{cm}^{-2}$ of low ionisation gas (logξ=-1.7$\pm$0.4). The relative abundances of the key elements, of C, N, O, Ne, Mg and Fe, were 0.7,0.9,0.20,0.75,1.0 and 1.0, though only O, Ne and Fe were well constrained in the fit. This best fit was obtained with a redshift of $\sim$0.1, implying the substantial column of 'cold' absorbing gas is local to 1H 0419-577. The power law slopes in the fit increased to $\Gamma\sim2.8$ (pn) and $\Gamma\sim2.7$ (MOS), while still leaving a further spectral steepening above ~3 keV (Figure 4c). Figure 4b illustrates the relevant XSTAR model, where the absorption structure is dominated by continuum absorption of C, O, Fe and Ne.

4.1. The form of the variable emission component

In the above spectral fit we assumed the variable emission component in 1H 0419-577 has the form of a power law. A similar conclusion was proposed from an *ASCA* study of the Seyfert 1 galaxy MCG-6-30-15 (Shih et al. 2002), and supported by extended *XMM-Newton* observations of the same source (Fabian and Vaughan 2003). However, it is notable that for 1H 0419-577 the power law fit including absorption (figure 4c) indicates further steepening above ~3 keV, and we recall the compTT model (Titarchuk 1994) gave an even better fit to the high state difference spectrum reported in Paper 1. Figure 5 reproduces the residuals to the single power law and a compTT fits to the high state difference spectrum. The thermal Comptonisation model has the additional appeal of being more physical than a power law fit. Since the intrinsic curvature of the thermal continuum might significally affect the derived absorption parameters we therefore repeated the analysis of the intermediate state difference spectrum with a model involving the emergence of an optically thick Comptonised emission modified by absorption in ionised matter.

Replacing the power law of section 4 with a Comptonised emission component, with an initial temperature of kT$\sim$2.7 keV and optical depth $\sim$4.4, as found for the high flux difference spectrum, the fit was indeed better than for the power law model, though still poor, with $\chi^2 = 1102/796$ dof and data:model residuals similar to those for the power law fit in figure 4a. Photoionised absorption represented by XSTAR was then added to the model. The outcome was a very good fit ($\chi^2 = 828/784$ dof) for an Comptonised emission component of kT=2.3$\pm$0.4 keV and optical depth 4.5$\pm$0.7. The absorption was again well modelled by low ionisation matter, with a column density of $N_H \sim 4.4 \times 10^{21} \mathrm{cm}^{-2}$ and ionisation parameter of logξ=-1.8$\pm$0.3. The relative abundances of the key elements, of C,N,O,Ne,Mg and Fe, were 0.2,0.2,0.12,0.4,0.7 and 0.66, with the lower abundances of C and N (compared with the power law fit) adjusting to the low energy curvature in the continuum fit.

Figure 6a shows the best-fit Comptonised emission component and pn camera data for the intermediate flux difference spectrum, with the XSTAR absorption component removed. Figure 6b reproduces the model spectrum while figure 6c illustrates the quality of the resulting fit.

5. Spectral fits to the mid-low flux state spectrum

Taken together with the high state difference spectrum reported in Paper 1, the above analysis of the intermediate state difference spectrum suggests the large scale spectral variability of 1H 0419-577 is indeed due to an emerging emission component which - at intermediate flux levels - bears the imprint of absorption by low ionisation matter. To see if that trend of variable absorption with flux level is continous, we repeated the above analysis for the mid-low flux state observation, starting with a 'conventional' power law plus blackbody fit.

Fitting a power law over the hard X-ray (2–10 keV) band yielded a photon index of Γ=1.41$\pm$0.03 (pn) and Γ=1.35$\pm$0.06 (MOS) for the mid-low flux spectrum. Statistically, the simple power law fit was good, with χ^2 of 68 for 71 dof. Extending this fit to 0.3 keV showed a soft excess rising sharply below $\sim$0.7 keV (figure 7a). The narrower profile of this soft excess (compared with that in figure 2a) allowed it to be well-modelled by the addition of a single blackbody component of kT $\sim$102 eV, no hotter blackbody being required. In this case a single absorption edge was needed to complete an excellent fit ($\chi^2 = 245/244$ dof). The edge was, however, deep ($\tau \sim 0.8$), and located at 0.76$\pm$0.01 keV. Figure 7b shows the ratio of data to this power law, blackbody and absorption edge model. In summary, a conventional fit to the mid-low flux spectrum of 1H 0419-577 shows a hard (flat) power law, with a sharply rising (cool) soft excess, and a deep absorption edge at $\sim$0.76 keV (in the

AGN rest frame).

The above fit provided a measure of the X-ray fluxes and luminosity of 1H 0419-577 in the the mid-low flux state, which were: 3.3×10^{-12} erg s^{-1} cm^{-2} (0.3–1 keV), 1.5×10^{-12} erg s^{-1} cm^{-2} (1–2 keV), and 8.3×10^{-12} erg s^{-1} cm^{-2} (2–10 keV), corresponding to a 0.3–10 keV luminosity for 1H 0419-577 of 2.8×10^{44} erg s^{-1} ($H_0 = 75$ km s^{-1} Mpc^{-1}).

Proceeding to examine the mid-low state difference spectrum, we followed the analysis procedure described in section 4, using compTT to model the emission component. The relatively poor statistics meant that the Comptonisation parameters were not well defined, the best fit having a temperature kT=2.1±1.5 keV and optical depth 2.7±2, while still failing to match the steeper fall-off at higher energies (figure 8c). However, the continuum fit was adequate to show the absorption trough to be noticeably deeper in the mid-low state difference spectrum (figure 8a). Fitting this absorption with XSTAR, with abundances fixed at the values found in the intermediate state model, again produced an acceptable fit (χ^2 = 259/238 dof), with a column density of $N_H \sim 2 \times 10^{22}$cm^{-2} and ionisation parameter of logξ=-2.3±0.3. While the ionisation parameters of the intermediate and mid-low difference spectra are the same within the formal errors, we see below that the lower ionisation in the mid-low flux state spectrum is critical to understanding the different shape of the absorption trough in the two spectra. Figure 8b reproduces the XSTAR model and figure 8c shows the data:model residuals for the mid-low difference spectrum fit.

6. The form of the variable absorption

The above difference spectrum fits indicate that absorption in low ionisation matter is substantially modifying the variable emission component - and hence the overall observed X-ray spectrum of 1H 0419-577; furthermore, we find the absorbing matter to become more ionised and the column density to fall as the continuum flux rises. To further explore the variable absorber we then computed the ratio of the 'raw' intermediate and mid-low flux spectra. The shape of that ratio plot (figure 9a) is particularly interesting, the marked drop observed at ~0.7 keV coinciding with low ionisation Fe absorption edges, with no obvious change in the flux ratio at the corresponding edges of low ionisation Oxygen. The flux ratio plot is thus consistent with the specific XSTAR models which match the relatively deeper absorption edge near 0.7 keV with the lower ionisation parameter for the lower flux state spectrum (cf figures 6b and 8b). A weaker feature at ~0.9 keV in figure 9a, close to the absorption edge structure of Ne, is also qualitatively consistent with the individual XSTAR fits. Figure 9b shows the ratio of the mid-high to high flux state spectra, indicating the same pattern of variable absorption feature continues as the flux level of 1H 0419-577 rises

towards the high state.

The different profile of the absorption in the intermediate and mid-low state difference spectral fits apparently determines - or is determined by - the changing ionisation parameter. To better understand that change we replot the key section of each XSTAR model fit in figure 10, where for ease of comparison with listed edges the energy axes are adjusted to the rest-frame of 1H 0419-577 and the principal absorbing ion stages are noted against the respective absorption features. Reference to the detailed absorption cross-sections for ground states of O and Fe (Kallman and Bautista 2001) then provides a qualitative explanation for the differential absorption we see in 1H 0419-577, since whereas the threshold energy cross-section in Fe increases by a factor $\sim$2.5 from FeV-FeI, the threshold cross-sections vary by only $\sim$40 percent from OIV-OI.

In summary, we find that the emerging emission component responsible for the main spectral change in 1H 0419-577 is modified by low energy absorption in a substantial column density of low ionisation matter. Further, while remaining low, the ionisation state of the absorber increases as the 1H 0419-577 gets brighter, while the absorbing column (or perhaps the covering factor) simultaneously decreases, and the increasing ionisation parameter provides a natural explanation of the changing energy profile of the absorption trough.

7. Spectral lines in the RGS data

Given the above evidence for substantial absorbing matter modifying the EPIC spectrum it is of obvious importance to check whether this is consistent with the higher resolution RGS data. To pursue that question we examined the simultaneous *XMM-Newton* grating data of 1H 0419-577, initially summing the data from all 5 orbits (512-690) to get the best statistics, since 1H 0419-577 is a relatively faint source. Figure 11 displays the RGS-1 and RGS-2 fluxed spectrum, binned relatively coarsely at 85 mÅ. The only spectral lines detected are all in emission, though the broad deficit between $\sim$10–20 Å is qualitatively consistent with the absorption trough seen in the EPIC spectra. The narrower absorption feature observed near 17.5 Å is also consistent with the Fe 2-3 UTA (Behar et al. 2001) indicated in the XSTAR model fits (fig. 10). The zero velocity wavelengths of the principal K-shell emission lines and radiative recombination continua (RRC) falling in the 8–38 Å waveband are indicated on the figure, and several are clearly detected.

To quantify the individual spectral features we modelled the RGS data with a simple power law fit, with $\Gamma\sim$2.45 yielding a reasonably good continuum fit ($\chi^2 = 4264/4084$) over the 8–38 Å band, and then added gaussians to each candidate emission line, in turn, with

wavelength, line width and flux as free parameters. 4 emission lines were formally detected, those of OVIII Lyα, the resonance and forbidden lines of the OVII 1s-2p triplet, and the forbidden line of NVI, together with the RRC of OVII. Table 1 lists the results. Interestingly, the gaussian line fits support the visible impression from the fluxed spectra that the profiles of the resonance lines of OVII and OVIII are resolved, the best fit line widths corresponding to a velocity width of 7000±3000 km s^{-1}.

Figure 12a shows the OVII and VIII lines at a higher resolution (35 mÅ bin width), and is compared in figure 12b with the same spectral region observed in the low state spectrum. Due to the much poorer statistics the latter fluxed spectrum is more coarsely binned, at 175 mÅ, and shows why only the OVIII Lyα and 0VII (f) lines were identified in the earlier analysis of the low state RGS spectrum (Paper 1). The improved statistics of the full spectrum now allows the OVII (r) line to be resolved, though the total line fluxes remain consistent with those observed in the low flux state (Paper 1).

8. Reconciling the RGS and EPIC spectra

The most important finding from our analysis of the EPIC spectra is of a substantial column density of low ionisation matter affecting the strongly variable emission component.

At first sight, the RGS data seem to be in conflict with the above picture, since no narrow absorption features are observed, even though the EPIC ratio spectra (figure 9b) shows significant broad band absorption remaining up to the mid-high flux state. However, we note the RGS is designed to detect emission and absorption lines, and is much less sensitive than EPIC to detecting continuum absorption. It is also possible that the absorbing material, if located close to the continuum emission region, is velocity broadened. In that context we note that the OVII and OVIII resonance emission lines are marginally resolved, suggesting an origin in moderately ionised matter with a velocity width of 7000±3000 km s^{-1}, while it is conceivable that a still higher velocity/ more turbulent outflow at smaller radii is responsible for the main absorption in the EPIC difference spectra. To check for absorption edge structure in the RGS data we subtracted the low state data from the summed spectra for March-June-September 2003, producing an intermediate state RGS difference spectrum, and plot that in Figure 13 against a simple power law model. With coarser binning (than in fig. 11) the plot is consistent with absorption edges similar to those found in the XSTAR fits to the intermediate state EPIC difference spectrum (fig. 6b), though the statistics are not good enough to usefully constrain any velocity broadened edges.

9. A re-appraisal of the Soft X-ray Excess

Modelling the soft excess (conventionally defined as the excess soft X-ray flux below above an extrapolation of the 2–10 keV power law) with one or more blackbodies, as in section 3, is a common practice in X-ray astronomy. However, since the implied blackbody temperatures are much higher than appropriate to an AGN accretion disc, a common explanation is that the disc photons gain energy by electron scattering in a hotter 'skin' or a 'corona' lying above the disc, though such Comptonisation models have remained rather ad hoc. Recently, a scaling by black hole mass of (more robust) Comptonisation models for Galactic black hole sources (Done and Gierlinski 2003) failed to explain the sharp upturn often seen below $\sim$1 keV in AGN spectra. Noting also the similar shape (or blackbody temperature) of soft excess in AGN over a wide luminosity range, those authors proposed that the soft excess in AGN could be an artefact of 'unseen or ignored' absorption (Gierlinski and Done, 2004).

The idea that absorption could be playing a larger part than normally assumed in shaping the broad band spectra of Seyfert 1 galaxies was put forward in an early mini-survey of *XMM-Newton* observations by Pounds and Reeves (2002). In figure 1 of Pounds and Reeves (2002) we showed the similarity in the 'observed' broad band spectra of AGN over a wide luminosity range, while noting that the more luminous sources exhibited a more 'gradual' onset of the soft excess. In comparing the present EPIC spectra of 1H 0419-577 we now find the same qualitative trend with flux level. Figure 14 compares the apparent soft excess above a 2–10 keV power law for the 5 flux states of 1H 0419-577, with the higher flux states showing a more 'gradual' (or hotter) soft excess. It is tempting to speculate that both trends are a function of the relative (to Eddington) accretion rate.

Our present analysis suggests that the 'conventional' soft excess is indeed strongly affected by absorption. The additional point to emphasise here is that the individual difference spectra, for high, intermediate, and mid-low states of 1H 0419-577 *exhibitnosoftexcess*. Instead, we identify a core $softX - rayemissioncomponent$ in the extreme low flux observation of September 2002 (Paper 1). Thermal emission from the accretion disc modified by scattering in a hotter skin or corona and reflection from a hot inner disc surface are possible contributors to this 'core' soft component. However, our present analysis of 1H 0419-577, with evidence for a substantial column of cold nuclear gas becoming less opaque as the X-ray flux increases, suggests that recombination emission from associated photoionised (outflowing?) matter is a natural origin of the soft excess. To test that idea we can compare the 'core' soft excess observed in the *XMM-Newton* low state observation of 1H 0419-577 with an emission model grid from XSTAR.

Figure 15a shows the 'soft emission component', obtained by removing the black body

and gaussian emission line attributed to a blend of the OVII triplet and OVIII Lyα from the broad band fit to the low flux state EPIC spectrum discussed in Paper 1. Quantitatively, the X-ray flux in that soft excess (0.3–2 keV) is $\sim 1.3 \times 10^{-12}$ ergs s^{-1}, some 30 percent of the flux removed by the low energy absorption trough in the intermediate flux state ('mean' ?) spectrum of 1H 0419-577. Replacing the blackbody and O-K emission components with a grid of photoionised emission models in XSTAR produced a statistically good fit (χ^2=1028/1058 dof), ie was able to reproduce the shape of the core soft emission, with an ionisation parameter log$\xi \sim 1.3$ and element abundances for C, N, O, Ne and Fe (relative to solar) of 0.4,0.4,0.15,0.35 and 0.45. We note the ratio of the key elements, O and Fe, suggests an over-abundance of Fe, similar to that found in the absorption modelling. Figure 15b reproduces the fitted XSTAR emission spectrum, showing how the emission profile, attenuated by the Galactic absorption in the line of sight to 1H 0419-577, matches the strongly peaked soft excess in figure 15a. It may also be understood, qualitatively, how the only lines detected in the full RGS spectrum of 1H 0419-577, velocity broadened in the figure by a gaussian width of $\sigma \sim 5$eV, are the principal emission lines of OVII, OVIII, NVI and CVI.

Finally it is interesting to compare the Fe K line in the model of figure 15b with the emission line detected in the intermediate flux state EPIC data (figures 2a and 3). Relative to the resonance lines of OVII and VIII the XSTAR model yields an Fe line which is a factor ~ 10 weaker, and is centered at ~ 6.42 keV (corresponding to FeXVII) compared with the EPIC line energy of 6.25 ± 0.12 keV. It seems probable, therefore, that the bulk of the observed Fe K line arises by fluorescence in low ionisation matter, with the absorbing column being an obvious candidate. In that case the observed line width and mean energy both indicate the re-processing matter lies within ~ 100 Schwarzschild radii of the SMBH.

10. Discussion

The analysis of 4 further *XMM-Newton* observations of 1H 0419-577 has produced 3 main results. First, our examination of the difference spectra of the intermediate and mid-low state EPIC data supports the conclusion in Paper 1 that the variable emission component has the form of a steep power law, or - a physically preferred - cool Comptonised thermal spectrum. Second, this variable emission continuum is modified at low energies by substantial absorption in low ionisation matter, the effect of which falls as the source flux increases. Third, we note that the X-ray luminosity 'lost' in the time-averaged absorbed flux is of the same order as that in the soft X-ray component seen in the low state spectrum of 1H 0419-577, reported in Paper 1, suggesting a natural origin of the 'core' soft X-ray emission.

It is important to note that the above analysis, modelling the difference spectra, assumes that the underlying hard power law and 'soft excess' seen in the low flux state in September 2002 remains constant - or, at least, much less strongly variable - over a timescale of 1–3 years. The similar power law index/ compTT parameters and absence of a soft excess in the mid-low, intermediate and high flux state difference spectra support that assumption and - in consequence - suggest the 'core' and variable X-ray emission components may have a separate origin. On the other hand, if the scenario we find is widely applicable to radio quiet AGN, it seems that these components must be coupled in some way in order to explain the 'canonical' power law index (neglecting reflection) of $\Gamma\sim1.7$ at 2–10 keV, observed in broad-band fits for Seyfert 1 galaxies in general, as well as the long-term average spectrum of 1H 0419-577.

The detection of absorption in the difference and flux ratio spectra of 1H 0419-577 indicates substantial low ionisation matter in the line of sight to the X-ray continuum emission. In turn the Seyfert 1 nature of 1H 0419-577 constrains the absorber to be closer to the black hole than the BLR or BBB emission region. The low ionisation parameter then requires the absorbing matter to be of high particle density ($\gtrsim10^{17}$ cm^{-3}) to survive so close to the continuum source. The rather dramatic variability in the absorbing column as the continuum flux changes is a further strong indication that it lies close to, or perhaps embedded in the emission region. It is possible that the absorbing matter is in clumps which partially cover the continuum source, the covering factor decreasing as the source flux increases, a change modelled by a reducing column density in our spectral fitting. Dense matter at the base of a jet or outflow, or corrugations in the accretion disc (Fabian et al. 2002) offer potential sites. The recent discussion of 'aborted jets', where dense blobs of matter are ejected from the inner accretion disc at sub-escape velocities (Ghisellini et al. 2004), also offers a geometry which might be compatible with the results we report here.

Although the spectral variability in 1H 0419-577 is extreme, it is notable that its low state X-ray spectrum is remarkably similar in appearance to the low state spectrum of the low luminosity Seyfert 1 NGC4051 (Pounds et al. 2004b, Uttley et al. 2004), and not unlike that of MCG-6-30-15 (eg Reynolds et al. 2004). In each case the hard power law continuum also exhibits a broad spectral feature at ~3–6 keV that may alternatively be fitted by an extreme relativistic Fe K line or by partial covering of the continuum by a substantial column of low ionisation matter. Conventionally the hard power law continuum is attributed to UV photons from the accretion disc being up-scattered in an overlying corona (eg. Haardt and Maraschi, 1991), with an unusually hard spectrum indicating a relatively low UV flux and 'photon-starved' corona. The intrinsic hardness of the 'core' spectrum would be reduced somewhat if continuum reflection is enhanced, for example by light bending in the strong gravity near the black hole, as proposed by Miniutti and Fabian (2004) to explain the extreme

Fe K emission line in the low state spectrum of MCG-6-30-15. In that case a simultaneous observation by *BeppoSAX* supported the enhanced reflection, rather than partial covering models. However, in the light of the new evidence reported here for substantial cold matter close to the black hole in 1H 0419-577 it is hard to exclude the possibility that absorption also modifies the strength and profile of the key diagnostic Fe K emission line in AGN spectra.

In seeking a physically distinct origin for the softer, variable component, several candidates arise. Thermal Comptonisation is strongly favoured as the emission mechanism by the excellent match to the high state difference spectrum. We also have evidence from simultaneous measurements of 1H 0419-577 with the Optical Monitor on *XMM-Newton* (Mason et al. 2001) that the UV (2120, 2910Å) flux increased by $\sim$20 percent from the low to the intermediate flux state (with smaller increases of $\sim$10 percent in the U band and $\leq$5 percent in V), consistent with the larger change in the UV between the high and low flux states (Paper 1). These data establish a link between the X-ray spectral change and enhanced thermal emission from the accretion disc. However, while increased disc emission could drive that change, the similarity in the luminosity increase in the soft X-ray and UV bands leaves open the alternative possibility that the UV flux increase is due to reprocessing of soft X-rays directed towards the (unobscured) outer disc. In the latter case the strengthening soft X-ray component would primarily be a consequence of an increased optical depth of Comptonising electrons. Though not well constrained, the steeper high energy slope of the difference spectra at lower flux levels provides some support for that view.

Given that the peak luminosity of the variable X-ray emission component is $\leq$10 percent of the bolometric (accretion) luminosity of 1H 0419-577 it is appealing to consider an origin linked with a wind or outflow. Although we have found no direct evidence for a massive outflow in 1H 0419-577 there is increasing evidence in other recent studies of AGN for ionised gas being driven out at velocities of $\sim$5–20 percent of c (Chartas et al. 2002, Pounds et al. 2003, Chartas et al. 2003, Reeves et al. 2003). It is also reasonable that any outflow will have an initial velocity which reflects the gravity of its origin (as with stellar winds) so that a wind emerging from a small radius will have a correspondingly high velocity. The kinetic energy carried by such a 'black hole wind' (King and Pounds 2003) could then support a separate emission mechanism of order v/c times the bolometric luminosity, with shocks in the outflow providing the enhanced Comptonising electrons. The apparent timescale of major spectral changes in 1H 0419-577 being of order several months suggest one possible cause of an increased outflow may be the co-alignment of magnetic field lines in the inner disc (Livio et al. 2001). Alternatively, if the variable X-ray emission arises from the base of a jet (eg. Markoff et al. 2001), then it is interesting to note that synchrotron radiation could - qualitatively - also explain the spectral form we see in 1H 0419-577.

The strong forbidden line of OVII is evidence that a substantial part of the 'core' soft X-ray emission comes from a region of relatively low density, where the emission measure then yields a radial extent (Paper 1) sufficient to maintain the soft X-ray emission essentially constant over the 3 years of our *XMM-Newton* studies of 1H 0419-577. The detection of a resolved resonance (1s-2p) line of OVII in the full RGS spectrum suggests an additional component to the soft X-ray emission from higher density gas closer to the continuum source. The comparable luminosity of the 'core' soft X-ray emission with the absorbed continuum in the intermediate (average) flux state then offers a natural explanation of the soft X-ray emission as an ionised outflow susequently recombines. The 'true' soft excess in Seyfert 1 galaxies, as we find for 1H 0419-577, may be more like the soft X-ray emission seen in Seyfert 2 galaxies, arising from an extended region of ionised gas.

11. Summary

1. A series of *XMM-Newton* observations of the luminous Seyfert 1 galaxy 1H 0419-577 has shown the large-scale spectral variability is primarily due to a steep power law or Comptonised thermal emission component of variable optical depth.

2. Broad absorption features superimposed on the variable emission continuum require substantial low ionisation matter apparently lying close to the central SMBH. As 1H 0419-577 brightens from a low to a high flux state the ionisation parameter increases and column density (or covering factor) of the absorbing matter falls.

3. An underlying assumption in our analysis is that a hard 'core' spectral component remains essentially unchanged over the 1–3 year period of the observations. We note the similarity of this 'core' X-ray spectrum of 1H 0419-577 to high quality 'low state spectra' of other Seyfert 1 galaxies, including NGC 4051 and MCG-6-30-15, which also show a flat power law, extreme Fe K emission line or partial covering, and strong 'soft excess'.

4. In the case of 1H 0419-577 we find the variable soft excess is essentially an artefact of continuum absorption, while a 'core' 'soft X-ray emission' component has a spectral form and luminosity consistent with re-emission of the absorbed X-ray continuum in an extended region of photo-ionised gas.

12. Acknowledgments

The results reported here are based on observations obtained with *XMM-Newton*, an ESA science mission with instruments and contributions directly funded by ESA Member

States and the USA (NASA). The authors wish to thank the SOC and SSC teams for organising the *XMM-Newton* observations and initial data reduction. KAP is pleased to acknowledge a Leverhulme Trust Emeritus Fellowship.

REFERENCES

Arnaud K.A., 1996, ASP Conf. Series, 101, 17

Behar E., Sako M., Kahn S.M., 2001, ApJ, 563, 497

Brissenden R.J.V. Tuohy I.R., Remillard R.A., Buckley D.A., Bicknell G.V, Bradt H.V, Schwartz D.A., 1987, PASAu, 7, 212

Chartas G., Brandt W.N., Gallagher S.C., Garmire G.P., 2002, ApJ, 569, 179

Chartas G., Brandt W.N., Gallagher S.C., 2003, ApJ, 595, 85

den Herder J.W. et al., 2001, A&A, 365, L7

Done C., Gierlinski M., 2003, MNRAS, 342, 1041

Fabian A.C., Ballantyne D.R., Merloni A., Vaughan S., Iwasawa K., Boller Th., 2002, MNRAS, 331, L35

Fabian A.C., Vaughan S., 2003, MNRAS, 340, L28

Ghisellini G., Haardt F., Matt G., 2004, A&A, 413, 535

Gierlinski M., Done C., 2004, MNRAS, 349, L7

Grupe D., Wills B.J., Leighly K.M., Meusinger H., 2004, AJ, 127, 156

Guainazzi M. et al., 1998, A&A, 339, 327

Haardt F., Maraschi L., 1991, ApJ, 380, L51

Kallman T. Liedahl D., Osterheld A., Goldstein W., Kahn S., 1996, ApJ, 465, 994

Kallman T., Bautista M., 2001, ApJS, 133, 221

Kaspi S., Smith P.S., Netzer H., Maoz D., Jannuzi B.T., Giveon U., 2000, ApJ, 533,631

King A.R., Pounds K.A., 2003, MNRAS, 345, 657

Laor A., 1991, ApJ, 376, 90

Livio M., Pringle J.E., King A.R., 2003, ApJ, 593, 184

Markoff S., Falcke H., Fender R., 2001, A&A, 372, L25

Marshall H.L., Fruscione A., Carone T.E., 1995, ApJ, 439, 90

Mason K.O,et al., 2001, A&A, 365, L36

Miniutti G., Fabian A.C., 2004, MNRAS, 349, 1435

Nandra K., Pounds K.A., 1994, MNRAS, 268, 405

Nelson C.H., 2000, ApJ, 544, L39

Page K., Pounds K.A., Reeves J.N., O'Brien P., 2002, MNRAS, 330, L1

Pounds K.A., Reeves J.N., 2002, in 'New Visions of the X-ray Universe in the *XMM-Newton* and *Chandra* era', ESA-SP XXX, Ed F.Jansen, (astro-ph/0201426)

Pounds K.A, Reeves J.N., King A.R, Page K.L, O'Brien P.T., Turner M.J.L., 2003, MNRAS, 345, 705

Pounds K.A., Reeves J.N., King A.R., Page K.L., 2004b, MNRAS, in press (astro-ph/0310257)

Pounds K.A., Reeves J.N., Page K.L., O'Brien P.T., 2004a, ApJ, 605, 670 (Paper 1)

Pye J.P. et al., 1995, MNRAS, 274, 1165

Reeves J.N., O'Brien P.T., Ward M.J., 2003, ApJ, 593, L65

Shih D.C., Iwasawa K., Fabian A.C., 2002, MNRAS, 333, 687

Strüder L.et al., 2001, A&A, 365, L18

Titarchuk L., 1994, ApJ, 434, 313

Turner T.J. et al., 1999, ApJ, 510, 178

Turner M.J.L. et al., 2001, A&A, 365, L27

Uttley P., Taylor R.D., McHardy I.M., Page M.J., Mason K.O., Lamer G., Fruscione A., 2004, MNRAS, 347, 1345

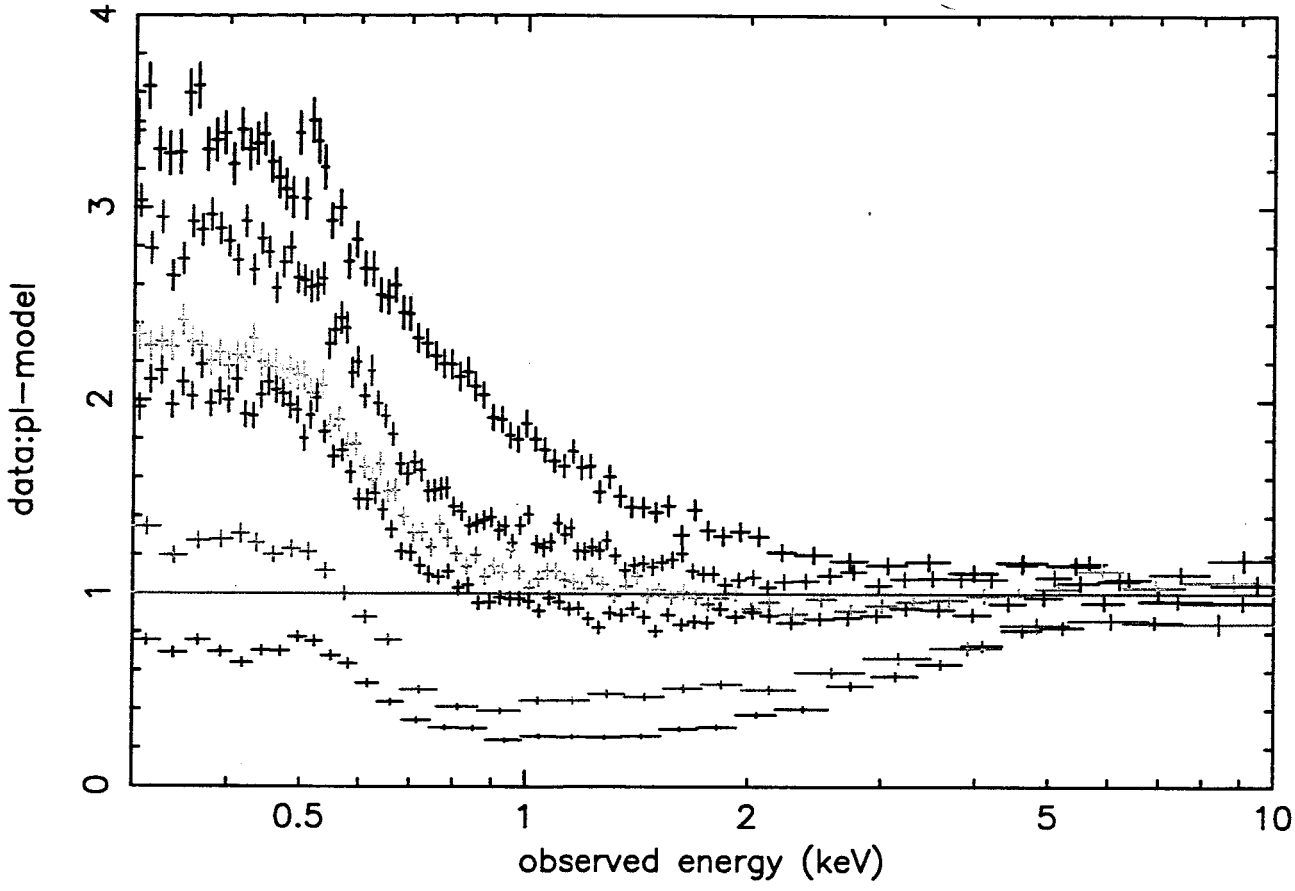

Fig. 1.— EPIC spectral data from the observations of December 2000, orbit 181 (black); September 2002, orbit 512 (red); December 2002, orbit 558 (green); March 2003, orbit 605 (dark blue); June 2003, orbit 649 (light blue); and September 2003, orbit 690 (magenta); compared (at 2–10 keV) with a power law of photon index Γ=1.73. For clarity only the pn camera data are shown.

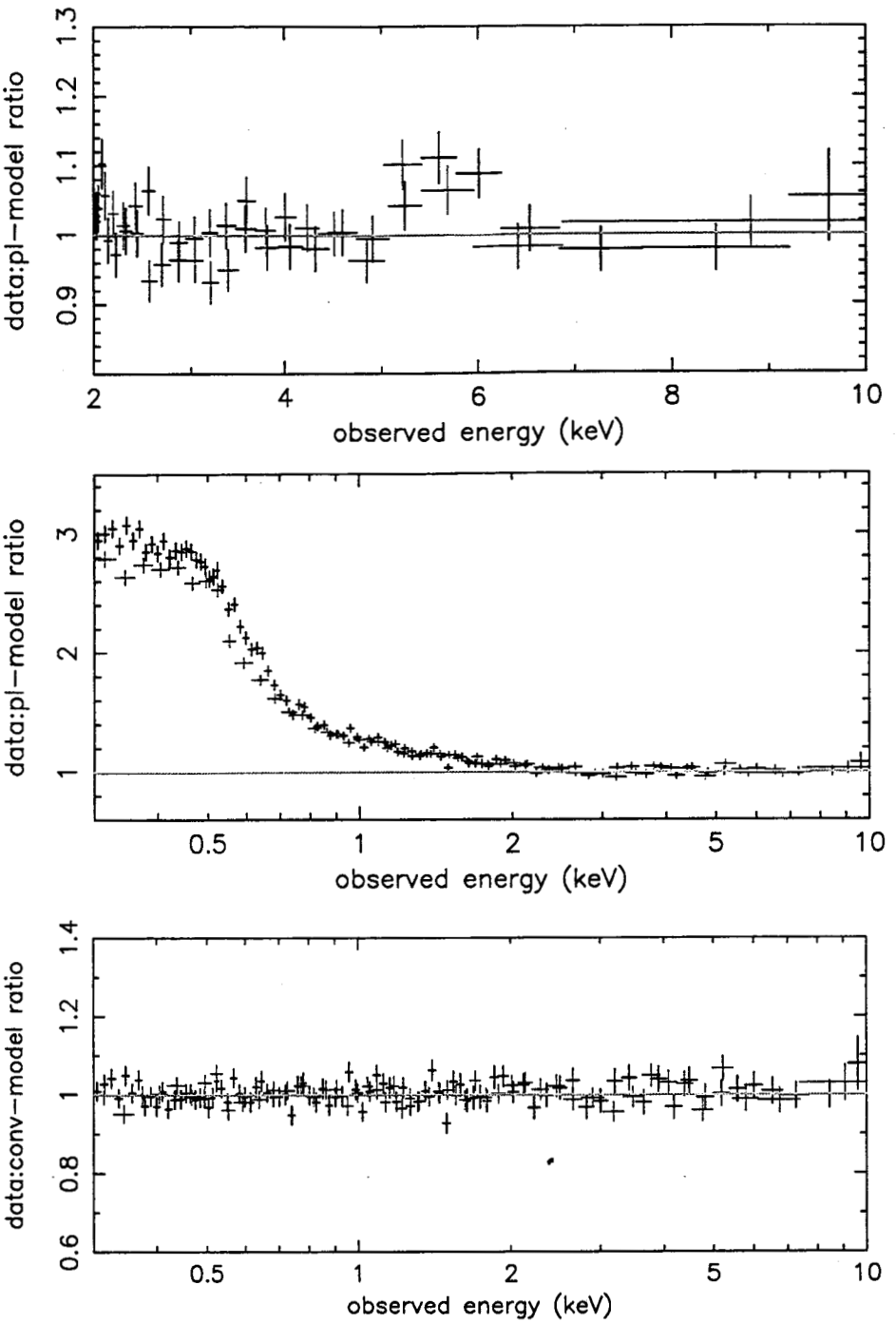

Fig. 2.— a.(top) Ratio of pn (black) and MOS data (red) to 2–10 keV power law fits to the intermediate flux state data (June/September 2003), showing a weak Fe K emission line. b.(mid) Extrapolation of 2–10 keV power law to 0.3 keV showing a strong soft excess. c.(lower) Ratio of data to conventional multi-component model spectrum described in section 3.

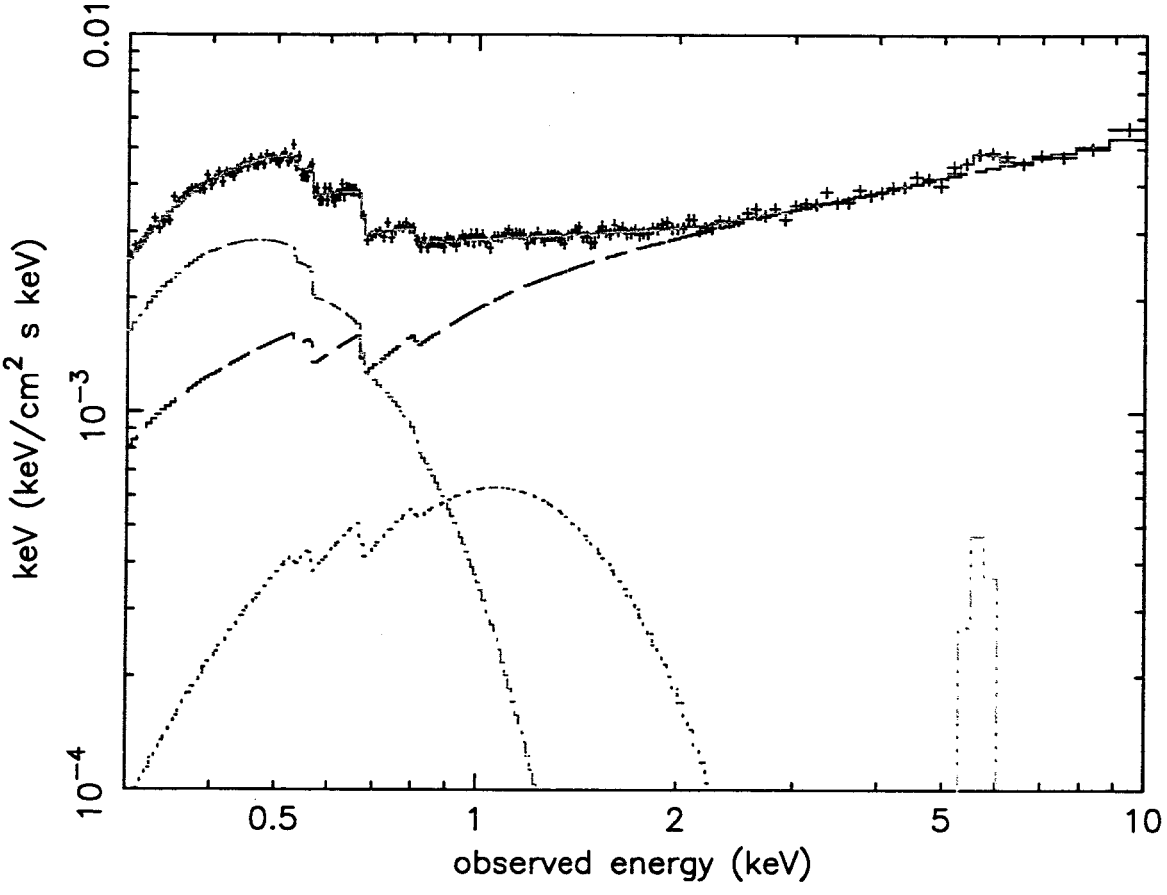

Fig. 3.— Unfolded broad band spectrum fitted to the intermediate flux state data for 1H 0419-577. The spectral components are: power law (red), blackbodies (dark blue and green) and Fe K emission line (light blue). For clarity only the pn data are shown.

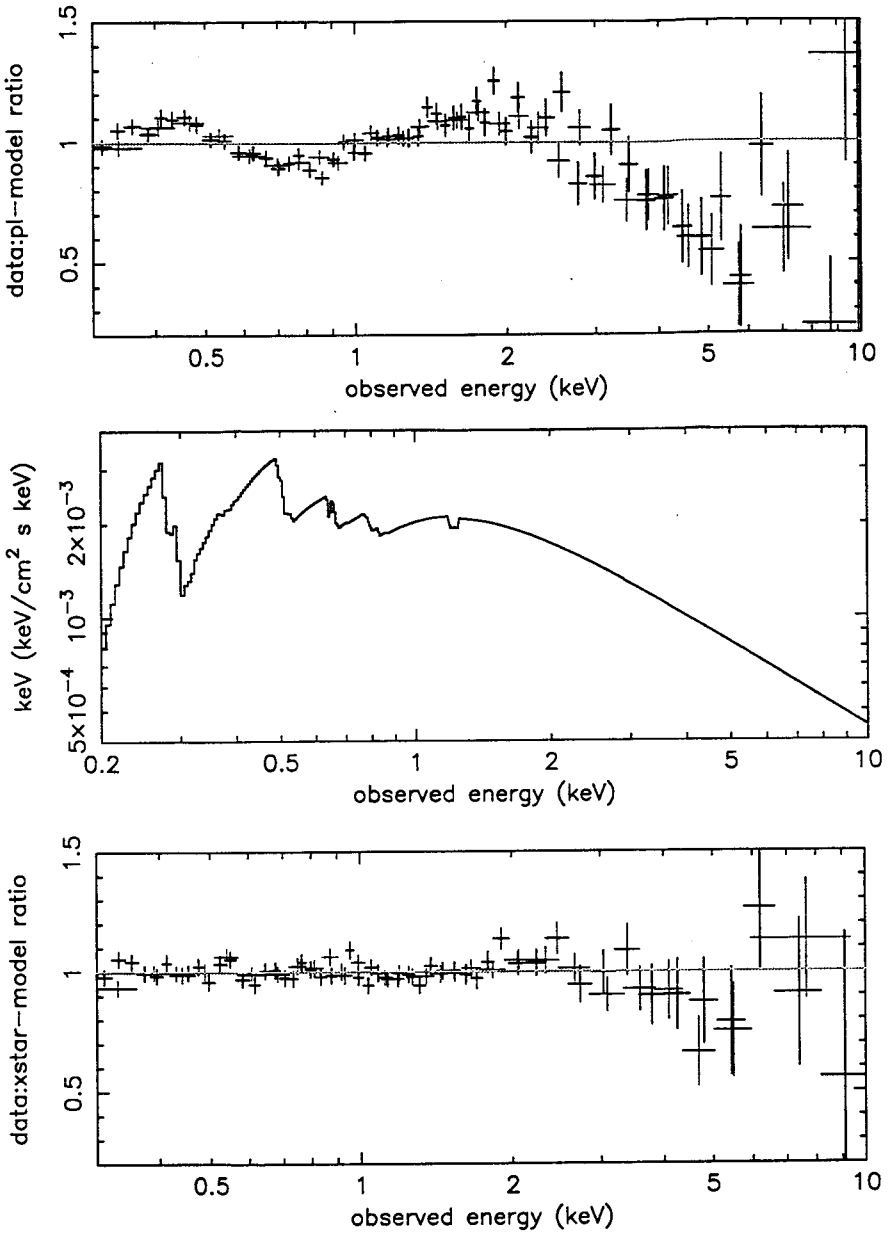

Fig. 4.— a.(top)Ratio of data to a single power law fit for the intermediate state difference spectrum. b.(middle)Power law plus XSTAR absorption model for the same difference spectrum, with strong absorption edge structure (in order of increasing energy) of C, O, Fe and Ne. c.(lower) Ratio of difference spectrum data to the power law plus absorption modelled in XSTAR. See section 4 for details.

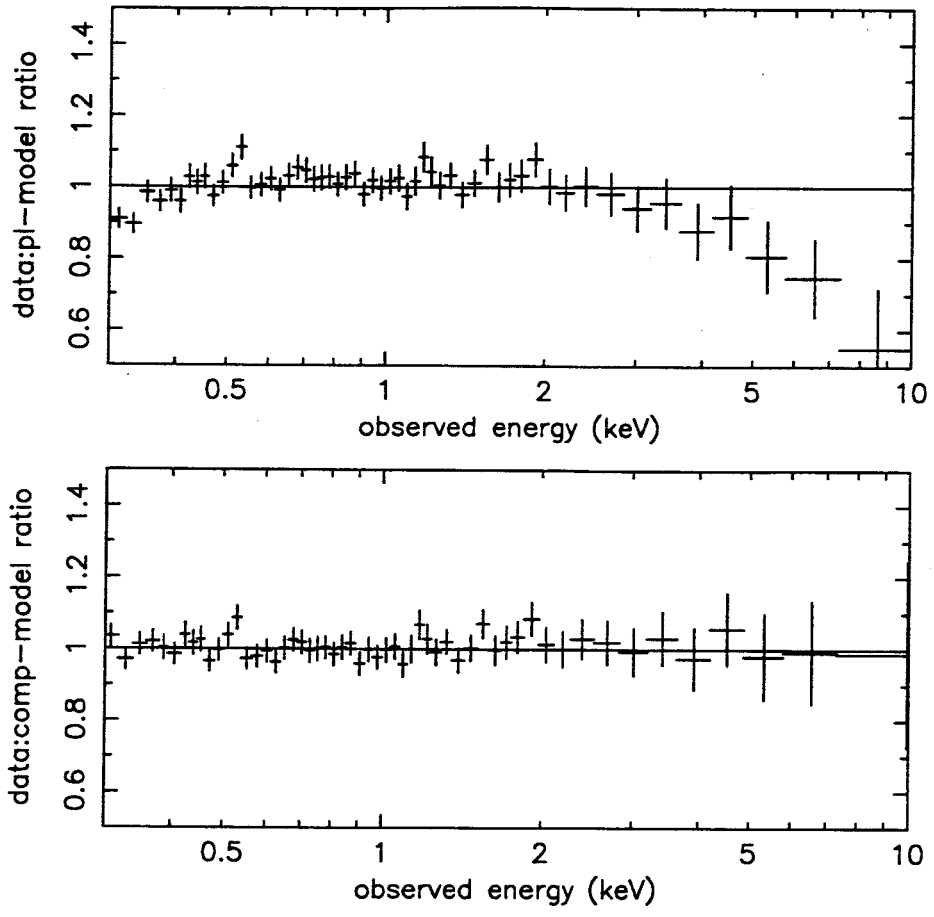

Fig. 5.— a.(top) Ratio of high state difference spectrum (December 2000) to a single power law model of photon index 2.47. b.(lower) Ratio of same data to a thermal Comptonisation model, with seed photons of kT=73±3 eV scattered in a plasma of temperature kT=2.7±0.6 keV and optical depth τ=4.4±0.6.

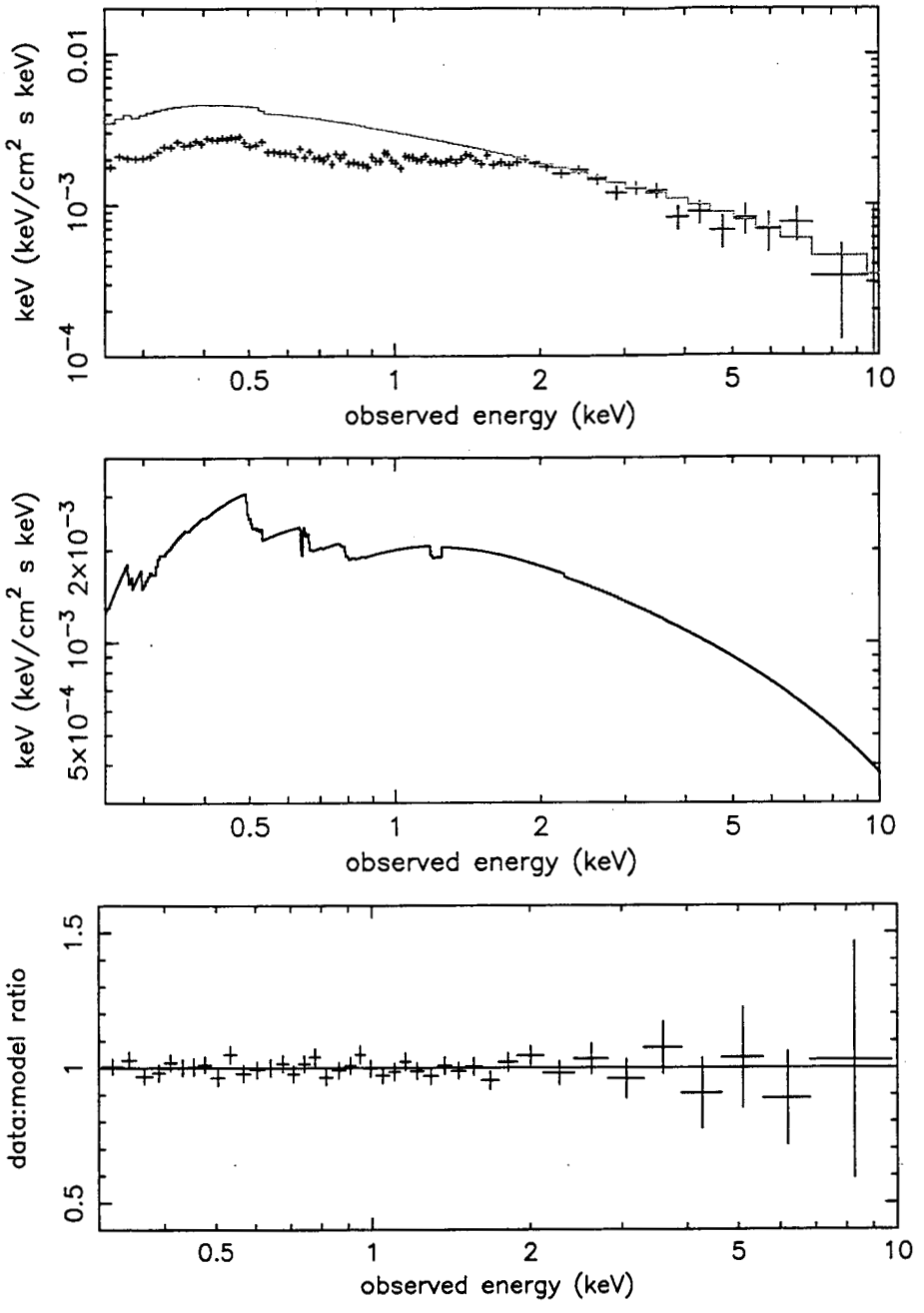

Fig. 6.— a.(top) Comptonised emission component and pn camera data for the intermediate state difference spectrum of 1H 0419-577. b.(mid) Comptonised emission plus XSTAR absorption model for the same data. c.(lower) Data to model ratio.

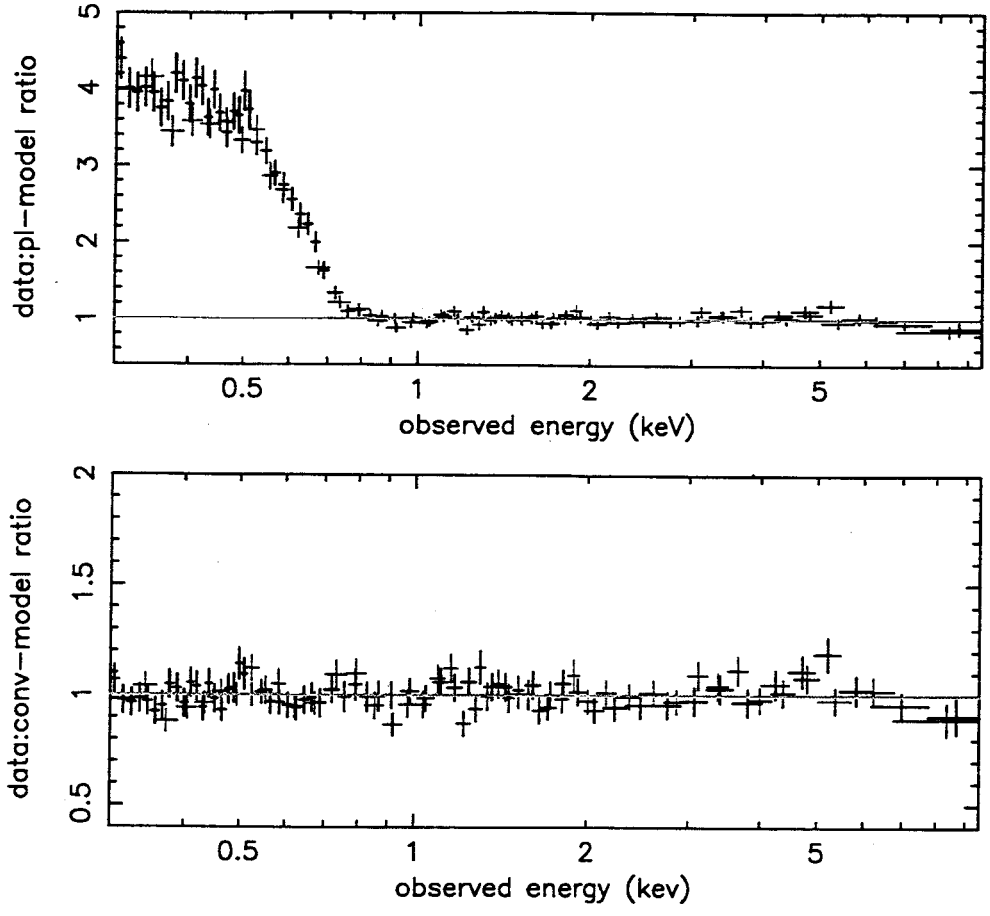

Fig. 7.— a.(top) Ratio of pn (black) and MOS data (red) to 2–10 keV power law fits to the mid-low flux state data (December 2002).. b.(lower) Ratio of data to conventional multi-component model spectrum described in section 5.

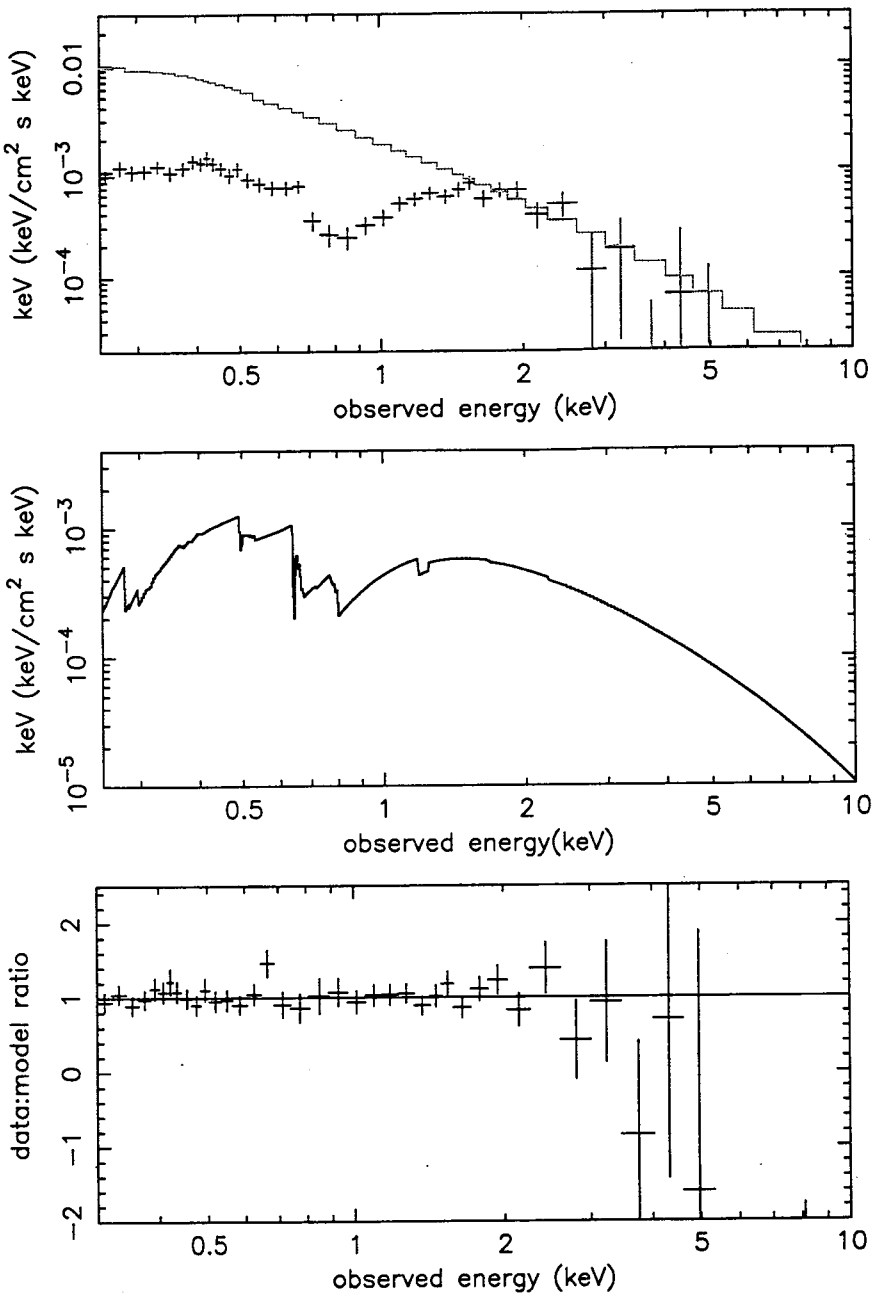

Fig. 8.— a.(top) Comptonised emission component and pn camera data for the mid-low state difference spectrum of 1H 0419-577. b.(mid) Comptonised emission plus XSTAR absorption model for the mid-low state difference spectrum. c.(lower) Data to model ratio.

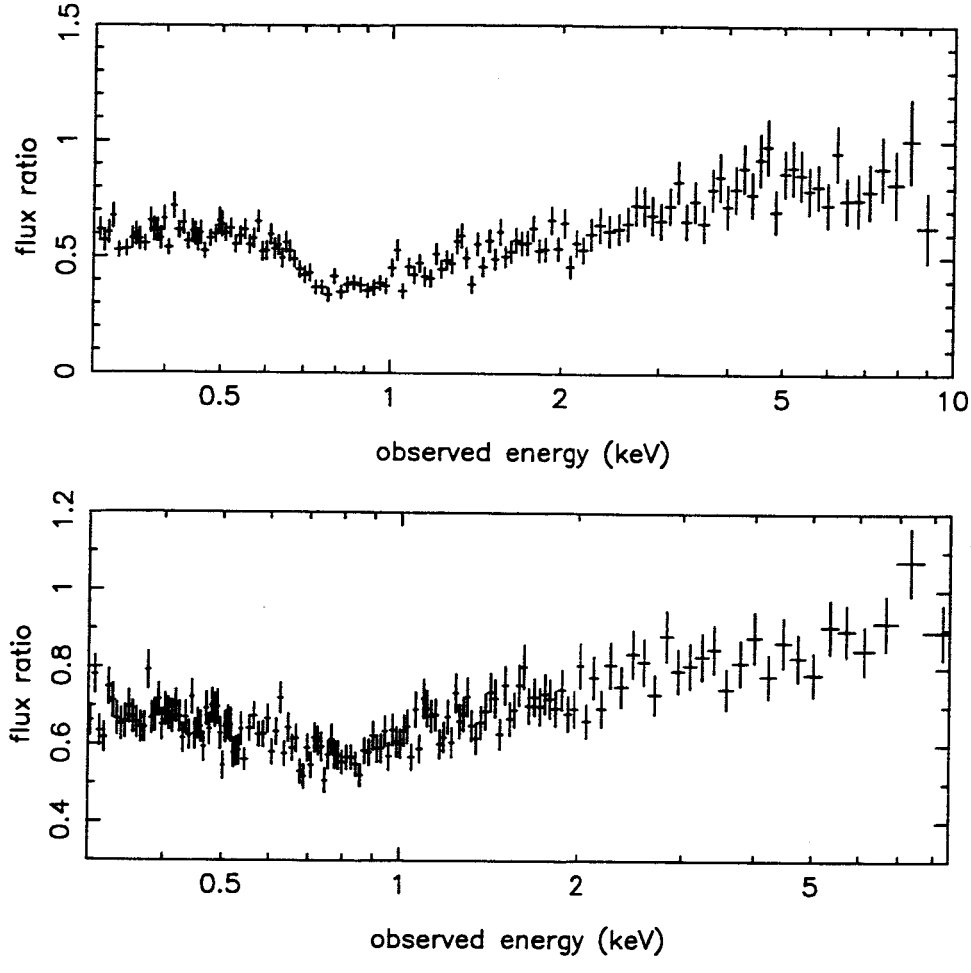

Fig. 9.— a.(top) pn camera data from the mid-low flux state observation divided by the data from the intermediate flux state observation. b.(lower) pn camera data from the mid-high flux state observation divided by the data from the high flux state observation.

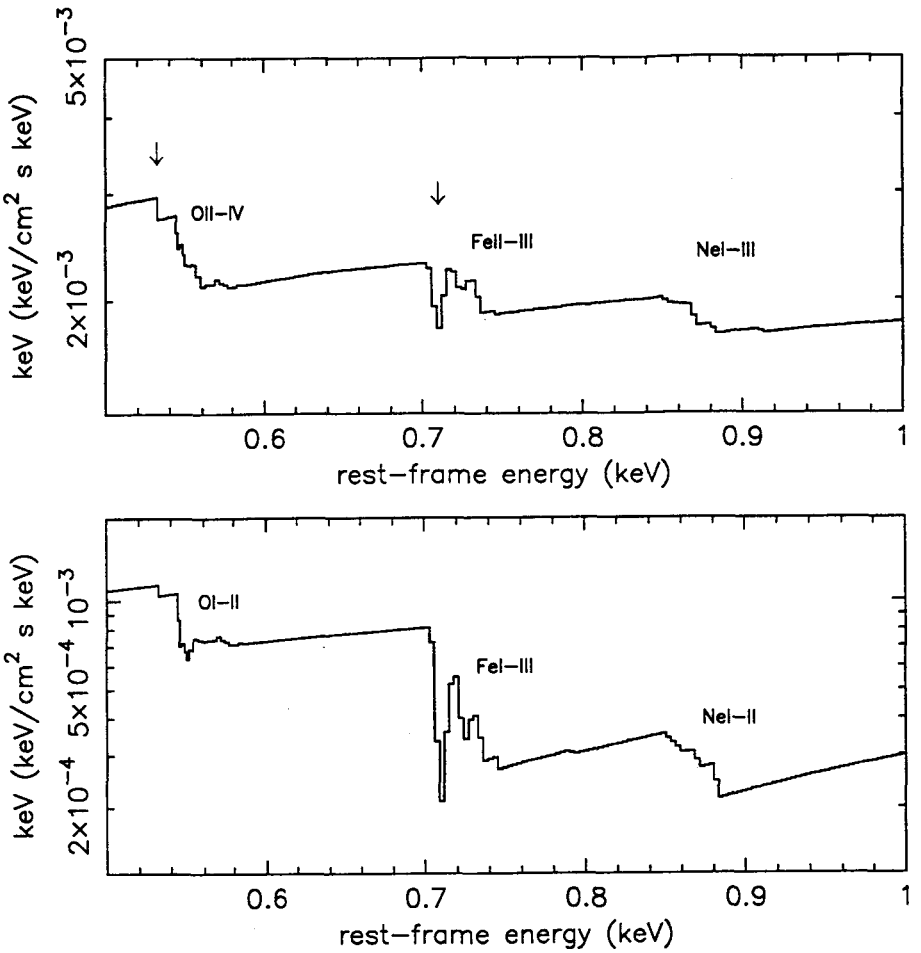

Fig. 10.— a.(top) Section of the compTT and XSTAR model fitted to the intermediate state difference spectrum showing the absorption edge structure in O, Fe, and Ne. The arrows note the OI edge due to the interstellar column in line-of-sight to 1H 0419-577 and the Fe 2-3 UTA. b.(lower) Same plot for the corresponding fit to the mid-low state difference spectrum. Both plots are adjusted to the rest-frame of 1H 0419-577.

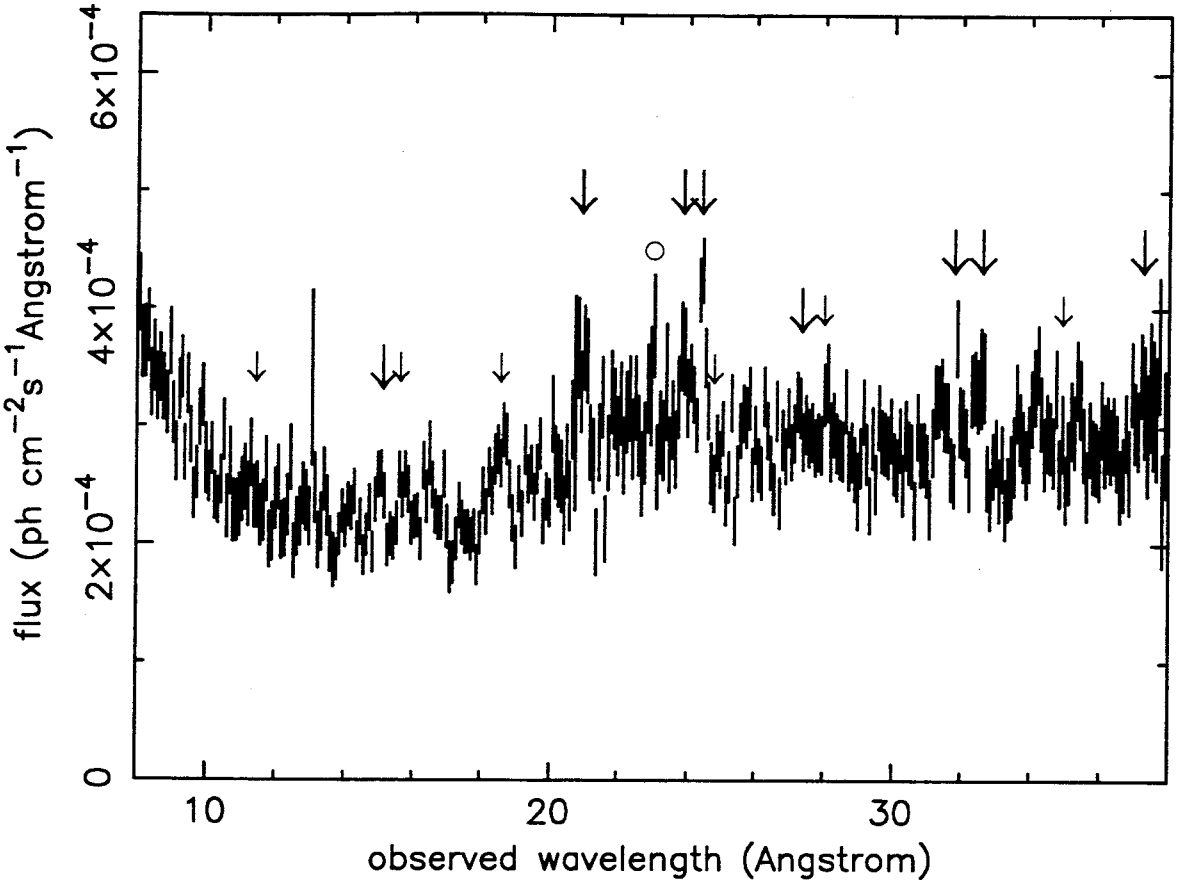

Fig. 11.— RGS spectrum of 1H 0419-577 summed over all 5 new *XMM-Newton* observations. The fluxed spectrum is binned at 85 mÅ resolution. Reading from left to right the larger arrows indicate the wavelengths of the principal candidate emission lines of NeIX (f), OVIII Lyα, OVII (r,f), NVII Lyα, NVI (r,f) and CVI Lyα, with the smaller arrows indicating the threshold wavelengths of the RRC of NeIX, OVIII, OVII, NVI, CVI and CV. The open circle at $\sim$23 Å notes a calibration defect.

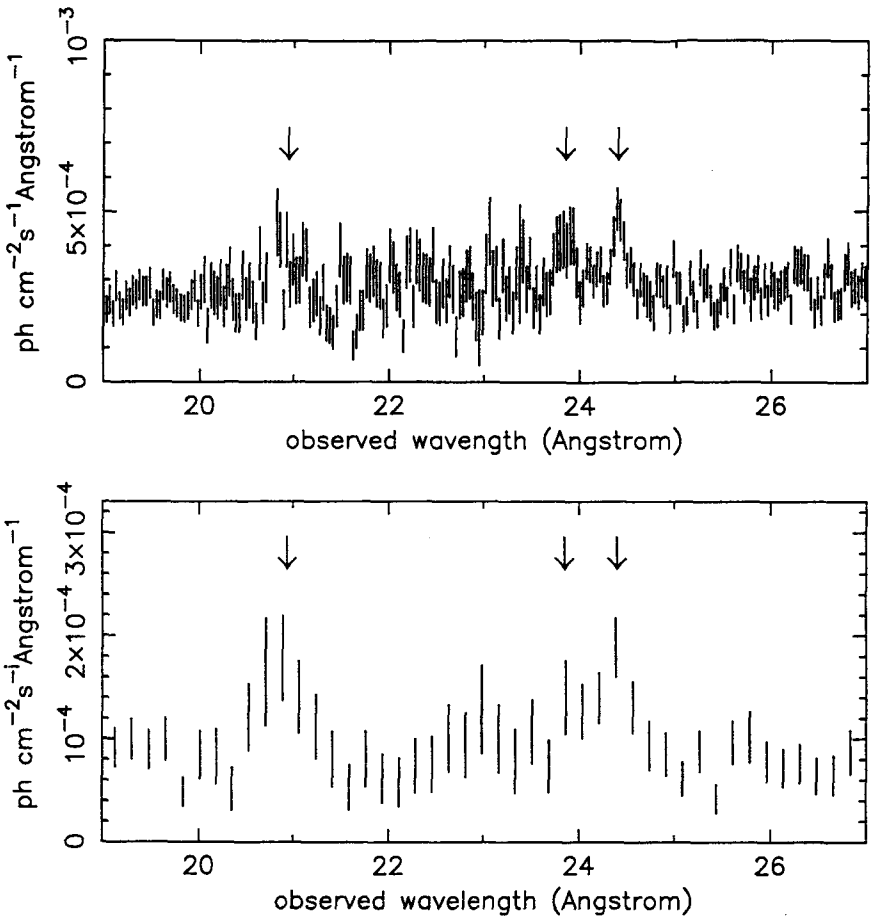

Fig. 12.— a.(top) Fluxed intermediate state RGS spectrum of 1H 0419-577 covering the waveband of OVIII Lyα and the OVII 1s-2p triplet binned at 35 mÅ resolution. b.(lower) The same spectral band from the low flux state observation of 1H 0419-577 binned at 170 mÅ resolution. The peak near 23 Å is due to imperfect modelling of the O-K absorption edge in the detector response function.

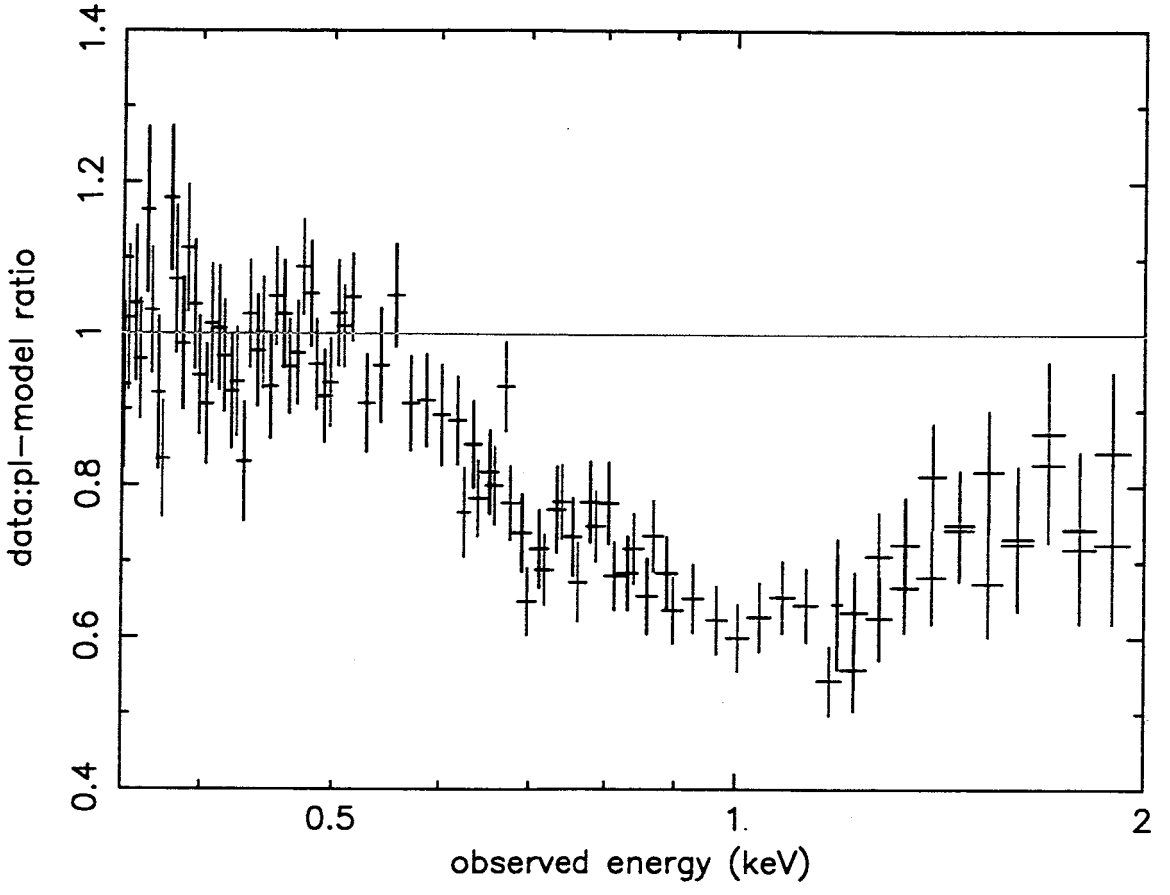

Fig. 13.— Coarsely binned RGS intermediate state difference spectrum of 1H 0419-577 plotted against a power law to illustrate absorption edge structures consistent with those seen in the simultaneous EPIC spectrum

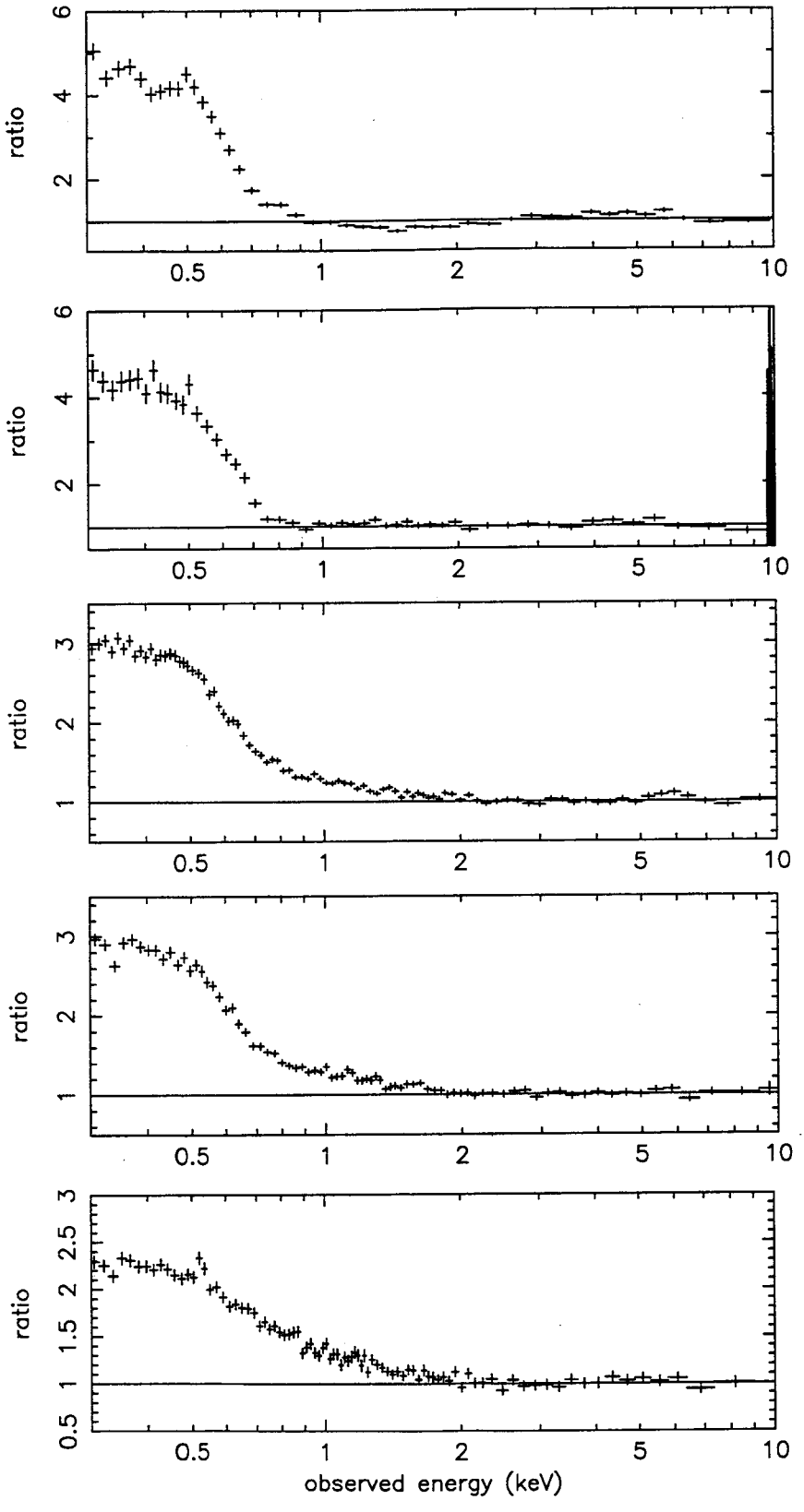

Fig. 14.— Reading from the top, the soft excess above a 2–10 keV power law fit for the low, mid-low, intermediate, mid-high and high flux states of 1H 0419-577.

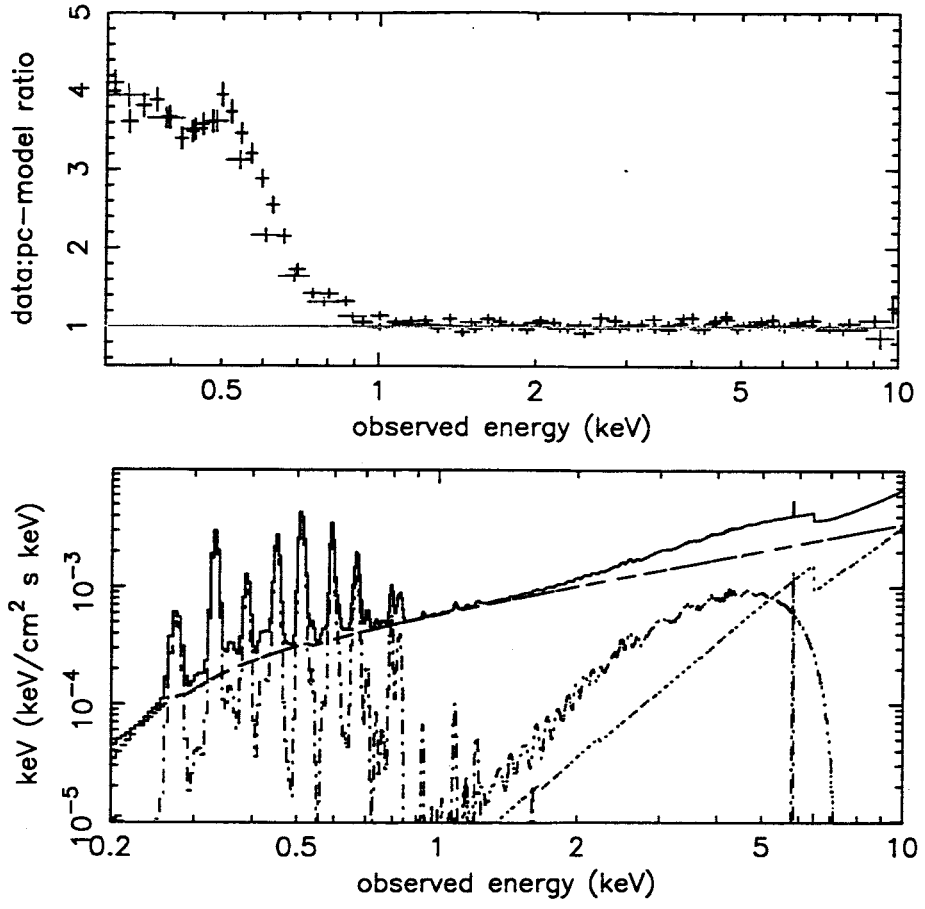

Fig. 15.— a.(top) Core soft excess obtained by subtracting the blackbody and 0.6 keV gaussian line components from the 0.3-10 keV power law plus laor line fit to the low state EPIC data. b.(lower) XSTAR emission spectrum replacing the blackbody and gaussian line components in an alternative fit to the core soft excess. Details are given in section 9.

Table 1: Identified lines in the RGS spectra

Feature	λ (Å)	σ/kT (eV)	Flux (10^{-5} ph cm^{-2} s^{-1})	EW (eV)	Δchi^2
OVIII Lyα	19.0	5 ± 2	6 ± 2	9 ± 3	22
OVII 1s-2p (r)	21.6	5 ± 2	6 ± 2	7 ± 2.5	22
OVII 1s-2p (f)	22.1	1 ± 1	4 ± 1.5	3.5 ± 1.2	32
NVI 1s-2p (f)	29.5	1 ± 1	5 ± 3	3 ± 1.5	14
OVII RRC	16.8	3.3 ± 1.8	1.9 ± 1.1	4 ± 2	18